

# Branching, Capping, and Severing in Dynamic Actin Structures

Ajay Gopinathan<sup>1</sup>, Kun-Chun Lee<sup>2</sup>, J. M. Schwarz<sup>3</sup> and Andrea J. Liu<sup>2</sup>

<sup>1</sup>*School of Natural Sciences, University of California, Merced,*

*CA 95344* <sup>2</sup>*Dept. of Physics and Astronomy, University of Pennsylvania,*

*Philadelphia, PA 19104* <sup>3</sup>*Dept. of Physics, Syracuse University, Syracuse, NY 13244*

(Dated: August 15, 2018)

Branched actin networks at the leading edge of a crawling cell evolve via protein-regulated processes such as polymerization, depolymerization, capping, branching, and severing. A formulation of these processes is presented and analyzed to study steady-state network morphology. In bulk, we identify several scaling regimes in severing and branching protein concentrations and find that the coupling between severing and branching is optimally exploited for conditions *in vivo*. Near the leading edge, we find qualitative agreement with the *in vivo* morphology.

When a cell crawls, it must reorganize the cytoplasmic network of biopolymers that controls its shape. The shape and motility of the leading edge (the lamellipodium) of a crawling cell are determined primarily by a dynamic network of actin filaments (F-actin) [1]. These filaments are living polymers made up of monomeric G-actin, and have a definite polarity such that monomers tend to be added to the plus (or “barbed”) end, and tend to fall off at the minus (or “pointed”) end. A host of regulatory proteins concentrate plus ends at the leading edge by controlling the morphology of the actin filament network [2]: capping proteins bind to the plus end of filaments, preventing further growth; severing proteins, such as cofilin, bind to filaments and break them in two, enhancing depolymerization; and the protein complex Arp2/3 nucleates branches from existing filaments, creating new plus ends at each branch tip and protecting the bound minus ends of branches from depolymerization. These proteins and their associated processes constitute the dendritic nucleation model [2]. This biological model is supported by experiments that show that severing, capping and branching are all crucial to cell motility [3, 4, 5, 6, 7].

In order to gain insight into how the cell controls its structural dynamics it is imperative to understand *quantitatively* how actin morphology can be controlled by the concentrations of these regulatory proteins. To date, theoretical studies of these kinetic processes have either omitted one or more of these critical processes [8, 9, 10, 11, 12] or have been restricted to describing just the overall amount of polymerization as a function of time [13]. Other treatments of actin-based motility have focused on the interplay of force generation with motility [14, 15], and treat the branched actin network either as an elastic continuum or as a collection of uncoupled filaments. In this paper, we adopt a complementary approach that not only captures all of the critical features of the dendritic nucleation model but also allows the first theoretical investigation of the morphology of the branched network. We confirm biological and biochemical understanding of the proteins involved by obtaining quantitative agreement with bulk *in vitro* experiments.

We extend the approach to explore the interplay between actin morphology and motility near the leading edge of a crawling cell. The agreement of our theory with electron microscopy images of the leading edge of a crawling cell provides strong evidence that the dendritic nucleation model captures the key players in this important form of cell motility.

We introduce a mean-field rate equation formulation for actin structures that undergo polymerization, depolymerization, capping, branching, and severing. We capture key morphological information by retaining the entire length distributions of filaments with free minus ends and of branches. Our formulation is constructed for polar actin assembly with branching (Arp2/3), severing (cofilin) and capping agents, whose action is described by rate constants. Initially, capping is taken into account by assigning a probability for a filament to be capped; for reversible capping, this renormalizes the polymerization rate. Thus,  $k_+$  is the effective polymerization rate constant. The growth rate at the barbed end of a filament is  $k_+\rho_m$ , where  $\rho_m$  is the free monomer concentration. The depolymerization rate is denoted by  $k_-$ . Nucleation and dissociation of filament seeds are described by rate constants  $k_n$  and  $k_d$  [16] respectively. Nucleation of branches is modeled by the rate constant  $k_{arp} = k_{arp}^0 \rho_{Arp2/3} \rho_m^2$  [12, 16], where  $\rho_{Arp2/3}$  is the concentration of Arp2/3. Eventually, Arp2/3 dissociates and branches detach at a rate  $k_{dr}$  [17]. Severing occurs at a rate  $k_s = k_s^0 \rho_s$ , where  $\rho_s$  is the severing protein concentration [18]. The nucleotide state of the polymerized actin controls the rates of both branching (preferred at ATP-actin sites[19]) and severing (preferred at ADP-actin sites[20]). We therefore consider hydrolysis and phosphate release occurring in sequence to convert newly polymerized ATP-actin to ADP-actin at a rate  $k_{pr}$  [21]. The probability that a monomer at distance  $L$  from the barbed end of a filament is an ADP-actin monomer is then given by  $p(L) = 1 - \exp(-L/l_c)$  [9], where  $l_c = k_+\rho_m/k_{pr}$ . We allow branching only on ATP-actin monomers and severing only on ADP-actin monomers in filaments.

Unless specified,  $k_+ = 8.7 \mu\text{M}^{-1}\text{s}^{-1}$  [22],  $k_- = 0.03 \text{s}^{-1}$  (estimates are of the order of  $10^{-2} - 10^{-1}$

[23] depending on conditions),  $k_d = 5 \times 10^{-4} s^{-1}$  [16],  $k_n = 3 \times 10^{-6} \mu M^{-1} s^{-1}$  (fitted; see caption of Fig. 1),  $k_{arp}^0 = 4.7 \times 10^{-4} \mu M^{-3} s^{-1}$  (fitted and consistent with [12])  $k_{dr} = 0.0018 s^{-1}$  [11, 12],  $k_s^0 = 4 \times 10^{-5} \mu M^{-1} s^{-1}$  (estimated from [18, 24]) and  $k_{pr} = 0.002 s^{-1}$  [25]. To capture the morphology we consider (1) the density of actin filaments of length  $L$  (in monomer units) with free

minus ends (*i.e.* minus ends that can depolymerize),  $\rho_u(L)$ , (2) the density of branches of length  $L$  (which have bound minus ends that cannot depolymerize),  $\rho_b(L)$ , and (3) the density of monomers,  $\rho_m$ . In the mean-field bulk case where all rate constants and densities have no spatial dependence, we have:

---


$$\begin{aligned} \dot{\rho}_u(L) = & -k_+ \rho_m (\rho_u(L) - \rho_u(L-1)) + k_- (\rho_u(L+1) - \rho_u(L)) + k_{dr} \rho_b(L) - k_s \sum_{L'=1}^{L-1} p(L') \rho_u(L) \\ & + \sum_{L'=L+2}^{\infty} k_s p(L) \rho_b(L') + \sum_{L'=L+1}^{\infty} k_s (p(L) + p(L'-L)) \rho_u(L') \end{aligned} \quad (1)$$

$$\dot{\rho}_b(L) = -k_+ \rho_m (\rho_b(L) - \rho_b(L-1)) - k_{dr} \rho_b(L) - k_s \sum_{L'=1}^{L-2} p(L') \rho_b(L) + \sum_{L'=L+1}^{\infty} k_s p(L'-L) \rho_b(L') \quad (2)$$

$$\dot{\rho}_u(2) = -k_+ \rho_m \rho_u(2) + k_- \rho_u(3) - k_d \rho_u(2) + k_{dr} \rho_b(2) + k_n \rho_m^2 + \sum_{L'=4}^{\infty} k_s p(2) \rho_b(L') + \sum_{L'=3}^{\infty} k_s \tilde{p}(L') \rho_u(L') \quad (3)$$

$$\dot{\rho}_b(2) = -k_+ \rho_m \rho_b(2) - k_{dr} \rho_b(2) + k_{arp} \sum_{L=2}^{\infty} \left( \sum_{L'=1}^L 1 - p(L') \right) (\rho_u(L) + \rho_b(L)) + \sum_{L'=3}^{\infty} k_s p(L'-2) \rho_b(L'), \quad (4)$$


---

with  $\tilde{p}(L') = p(2) + p(L'-2)$ . A fifth equation is the conservation of total number of monomers. These equations are similar to those in Refs. [10, 11, 12, 13], though we distinguish between unbranched and branched filaments, which is necessary to quantitatively describe morphology.

We first study the steady state in absence of severing and nucleotide dependence. The length distributions are

$$\rho_u(L) = A e^{-L/\lambda_u} + B e^{-L/\lambda_b} \quad (5)$$

$$\rho_b(L) = C e^{-L/\lambda_b} \quad (6)$$

where  $\lambda_u = 1/\log \frac{k_-}{k_+ \rho_m} \approx \frac{k_+ \rho_m}{k_- - k_+ \rho_m}$ ,  $\lambda_b = 1/\log \frac{k_{dr} + k_+ \rho_m}{k_+ \rho_m} \approx \frac{k_+ \rho_m}{k_{dr}}$ .  $A, B$  and  $C$  are length-independent and depend on the rate constants and total actin concentration. The approximations are valid for  $L \gg 1$ , which is generally the case *in vivo*, and imply that  $k_- \approx k_+ \rho_m$  and  $\lambda_b = k_+ \rho_m / k_{dr} \approx k_- / k_{dr}$ .

We performed Brownian dynamics simulations to determine the accuracy of Eqns.(5,6) [26]. We have used rates somewhat different from physiological ones to achieve equilibration within reasonable time. Fig 1(a) shows that the simulations and theory yield length distributions in good agreement with each other with no adjustable parameters at these concentrations. The predicted maximum in  $\rho_u(L)$ , which occurs because branches can fall off, is also observed in the simulations.

We have also compared our calculations to *in vitro* experiments by Blanchoin, *et al.* [27]. We neglect severing, depolymerization and nucleotide-state dependence because those experiments did not contain severing pro-

teins and filaments were stabilized by phalloidin. Our results for the barbed end concentration are plotted as a solid curve as a function of Arp2/3 concentration in Fig. 1(b), in good agreement with the experiment.

When severing and monomer nucleotide state are included, analytical progress can be made by using “global” conservation principles at steady state to derive simple, approximate expressions for morphological properties. In steady state, the average total number of branches must be conserved. Equating the rate of production and destruction of branches gives  $k_{dr} \sum_{L=2}^{\infty} \rho_b(L) = k_{arp}^0 \rho_{Arp2/3} \rho_m^2 \sum_{L=2}^{\infty} (\sum_{L'=1}^L (1 - p(L'))) (\rho_u(L) + \rho_b(L)) \approx k_{arp}^0 \rho_{Arp2/3} f (\frac{k_-}{k_+})^2 \rho_m^{tot}$ , where  $\rho_m^{tot}$  is the total actin concentration and  $f$  denotes the fraction of polymerized F-actin monomers that are ATP-bound and hence capable of supporting branching and immune to severing.

Similarly, the average number of free filaments is fixed such that  $k_s (1 - f) \sum_{L=2}^{\infty} L (\rho_u(L) + \rho_b(L)) + k_{dr} \sum_{L=2}^{\infty} \rho_b(L) = k_d \rho_u(2)$ . If we assume that  $\rho(L)$  can be described by one characteristic length,  $\bar{L}_u$ , implying  $\rho_u(2) \approx \rho_m^{tot} / \bar{L}_u^2$ , then  $\bar{L}_u = \left( \frac{k_d}{k_s (1-f) + k_{arp}^0 \rho_{Arp2/3} f (\frac{k_-}{k_+})^2} \right)^{\frac{1}{2}}$ . In steady state, conservation of ATP F-actin implies  $f \approx (k_{pr} \frac{\bar{L}_u}{k_-} + 1)^{-1}$  such that

$$\bar{L}_u \simeq \left( \frac{k_d (k_{pr} \bar{L}_u + k_-)}{k_s k_{pr} \bar{L}_u + k'_{arp} (\frac{k_-}{k_+})^2 k_-} \right)^{\frac{1}{2}}, \quad (7)$$

where  $k'_{arp} = k_{arp}^0 \rho_{Arp2/3}$ . Comparing the two terms in the denominator, we see that branching does not sig-

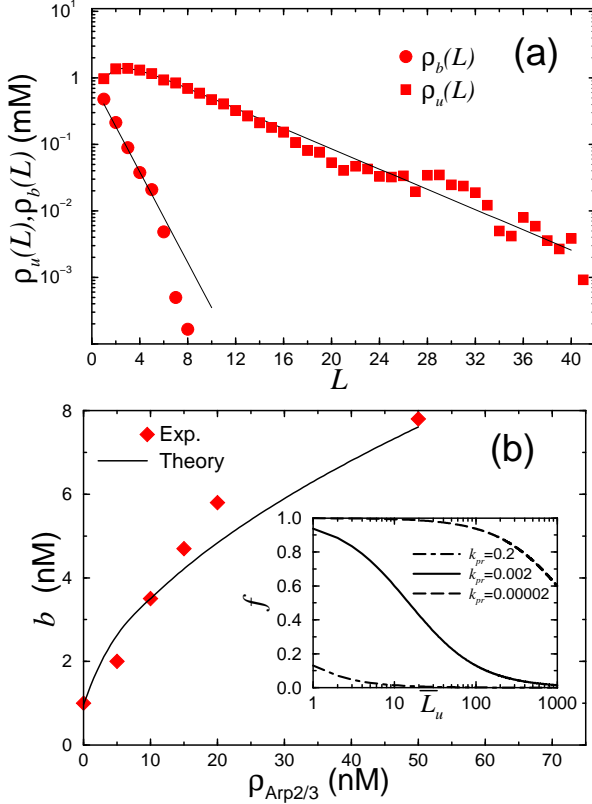


FIG. 1: (a) Length distribution of filaments and of branches (in monomer units), as predicted by our mean field theory (lines) and as calculated from Brownian dynamics simulations (points), with  $k_+ = 15 \mu M^{-1} s^{-1}$ ,  $k_- = k_{dr} = 100 s^{-1}$ ,  $k_{arp}/k_+ = 0.015$ . (b) The barbed end concentration as a function of  $\rho_{Arp2/3}$ , as predicted by mean field theory (lines) and measured by experiment (points) [27]. Here,  $k_n$  and  $k_{arp}^0$  were estimated by fitting to average filament length and branching percentage data from [27] (not shown). Inset: The predicted steady-state value of the fraction of ATP-bound actin monomers in filaments, as a function of  $\bar{L}_u$  for various  $k_{pr}$  in units of  $s^{-1}$ .

nificantly affect the average length  $\bar{L}_u$  until the Arp2/3 concentration,  $\rho_{Arp2/3}$ , is at least four orders of magnitude larger than the cofilin concentration,  $\rho_s$ . *In vitro* motility experiments [3] typically operate in the regime where  $\rho_{Arp2/3} < \rho_s$ . Then Eq. 7 shows that for large  $k_s$ ,  $\bar{L}_u$  is short and scales as  $\bar{L}_u \sim (k_d k_- / (k_s k_{pr}))^{1/3}$ . For lower  $k_s$ , (but  $k_s \gg k'_{arp} (\frac{k_-}{k_+})^2$ ),  $\bar{L}_u$  is larger and shows a more sensitive dependence on  $k_s$ :  $\bar{L}_u \sim (k_d / k_s)^{1/2}$ . The crossover between these two regimes occurs when  $\bar{L}_u \sim 10$ . On the other hand, when severing is negligible and  $k_{pr}$  is small such that side-branching dominates, then  $\bar{L}_u \propto 1 / \sqrt{k'_{arp}}$ . For small  $k_s$  and large phosphate release rates  $k_{pr}$ , where end-branching dominates,  $\bar{L}_u \propto 1 / k'_{arp}$ . These scaling predictions are experimentally testable.

The density of branched filaments is also constant in steady state. As  $k_{pr}$  increases, branching occurs only near the barbed end of filaments. Thus, the branch density will depend not on the number density of monomers

in filaments, but on the number density of *filaments*, which is sensitive to severing and is given by  $\sum \rho_b \propto \sqrt{k_s k'_{arp}}$ . On the other hand, if there is no dependence on nucleotide state, the branch density depends on the total F-actin concentration, which depends on  $k'_{arp}$ , but not sensitively on  $k_s$ .

These results suggest that the dependence of branch density on the nucleotide state of filament monomers allows the cell to control morphology by varying the concentration of severing protein [13]. For *in vivo* values of  $k_{pr}$ , the system switches from a side-branching regime ( $f = 1$ ) to an end-branching regime ( $f = 0$ ) as the average lengths increase from tens to several hundred subunits, the range typically observed *in vivo*. In Fig. 1(b), we plot the predicted value of  $f$  as a function of average filament length for different values of the phosphate release rate. For the *in vivo* value of the phosphate release rate and the *in vivo* range of filament lengths (ranging from tens to several hundreds of monomers), the range of  $f$  that is covered is almost maximal. This suggests that *in vivo*, the branching morphology (controlled by  $f$ ) is maximally sensitive to severing proteins. Branching and severing have been viewed as antagonistic, because branching promotes filament growth and severing promotes depolymerization. However, our results show that all processes combine to give maximal cooperativity between branching and severing.

We now consider the coupling of morphology to motility by confining the system between two hard walls both moving with velocity  $v$ . The “front” wall models the leading edge of the cell and while the “back” wall denotes the back edge of the lamellipodium. Because capping is necessary to motility [7], we extend Eqns. (1-4) to explicitly include a capping rate  $k_c$  and uncapping rate  $k_{uc}$  by defining four populations of filaments: capped and uncapped branched and unbranched filaments. Now  $\rho_u(L, t, z)$  denotes the density of capped or uncapped filaments of length  $L$  whose barbed ends are at distance  $z$  from the front wall. Experiments find that filaments are typically at an angle of  $\theta = 35^\circ$  with respect to the leading edge [28], so we assume that all filaments are at that angle with the wall. Because Arp2/3 is activated at the leading edge and diffuses away from it, we model the Arp2/3 concentration profile as an exponential decay from the front with a decay length  $z_{arp}$  [29]. Similarly, we use a severing concentration profile that is an inverted exponential with a rise length of  $z_s$  to model the effect of nucleotide dependence on the severing efficiency. Finally, the amount of free monomers is determined by the conservation of actin, and actin that flows beyond the back wall is recycled in as free monomers; our results are for systems sufficiently large such that actin reaching the back wall is small compared to actin within the system. We use an exponential profile with a decay length of  $D/v_t$ , consistent with the diffusion equation, where  $D$  is the diffusion constant of free monomers and  $v_t$  is the

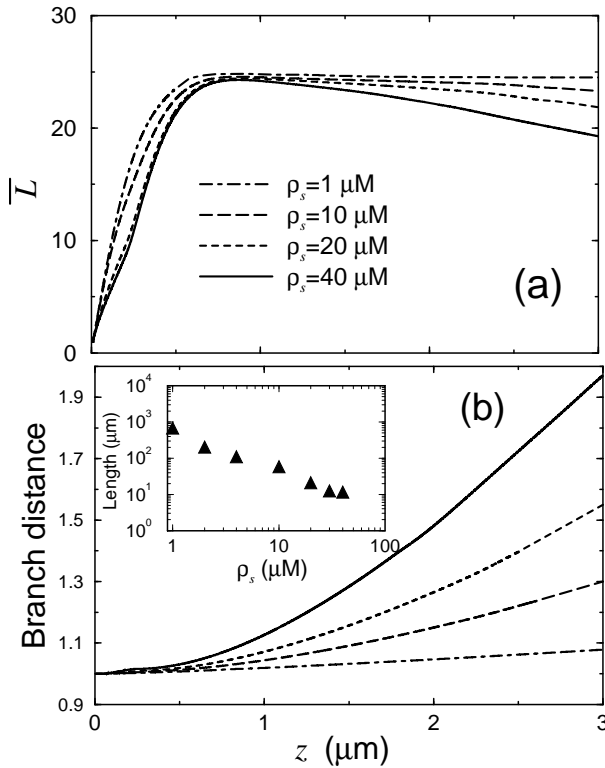


FIG. 2: (a)  $\bar{L}$  vs. distance from leading edge,  $z$ , for different cofilin concentrations,  $\rho_s$ . Here,  $v = 0.1 \mu\text{m}/\text{min}$ ,  $v_t = 25 \mu\text{m}/\text{s}$ ,  $D = 5 \mu\text{m}^2/\text{s}$ ,  $z_{arp} = 0.1 \mu\text{m}$ ,  $z_s = 2 \mu\text{m}$ ,  $k_c = 1 \text{s}^{-1}$ ,  $k_{uc} = 0.01 \text{s}^{-1}$  with  $1 \mu\text{M}$  Arp2/3 and  $100 \mu\text{M}$  actin (at the upper end of the physiological range). (b) Distance between branches vs.  $z$  for the same  $\rho_s$  as in (a). Inset: Lamellipodium length vs.  $\rho_s$ .

transport (bias) velocity of free monomers towards the surface. We choose  $v_t = 250v$ , where  $v$  is the speed of the moving surface, consistent with results of Zicha *et al.* [30]. Not all values of  $v_t$  yield reasonable morphologies. If, for example,  $v_t = 500v$ , the system tends toward a state with no filaments.

In steady-state, we find that branching, severing, and capping are all needed to obtain a morphology that is consistent with experiments. Branching in the front is needed to help the system “keep up” with the wall by nucleating new filaments. Capping towards the front channels new filament growth into shorter branches and thus increases filament density. Finally, severing is needed to replenish the free monomer supply. Fig. 2 shows the steady state morphology for the system with a moving surface. In Fig. 2(a), we plot the average length of filaments (branched and unbranched) as a function of distance  $z$  from the front wall. The average length,  $\bar{L}$ , is short near the surface, and increases to approximately  $100 \text{ nm}$  at a distance of roughly  $0.5 \mu\text{m}$  from the surface. As the severing protein concentration  $\rho_s$  increases,  $\bar{L}$  decreases with increasing  $z$ , eventually reaching zero when all filaments are depolymerized away. The distance at which  $\bar{L}$  reaches zero provides an upper bound on the

lamellipodium length, *i.e.* the distance the lamellipodium extends into the cell from the leading edge. This length is plotted in the inset to Fig. 2(b) as a function of  $\rho_s$ . For tens of micromolar concentrations, the lamellipodium length is tens of microns, consistent with experimental observations [31]. The predicted length increases with actin concentration.

Fig. 2(b) shows that the average distance between branches monotonically increases with  $z$ . The higher  $\rho_s$ , the greater the increase in the branch distance with  $z$ . In short, Fig. 2 implies that the morphology consists of short branched filaments within the first micron of the leading edge, with longer, less branchy filaments further away. These observations are consistent with electron microscopy images of the lamellipodium in crawling keratocytes [31], suggesting that the dendritic nucleation model captures the minimal set of proteins involved. A thorough, quantitative experimental test of our results near a moving surface should provide a stringent check on the validity of the dendritic nucleation model for actin assembly near the leading edge of a crawling cell.

We thank T. Svitkina for instructive discussions and are grateful for support from NSF-CHE-0613331 and NSF-DMR-0520020.

- [1] H. Lodish, *et al.*, *Molecular Cell Biology*, 3rd ed., (W. H. Freeman, New York, NY, 1995).
- [2] T. D. Pollard, *et al.*, *Annu. Rev. Biophys. Biomol. Struct.* **29**, 545 (2000).
- [3] D. Pantaloni, *et al.*, *Science* **292**, 1502 (2001).
- [4] A. Y. Chan, *et al.*, *J. Cell. Biol.* **148**, 531 (2000).
- [5] M. Bailly, *et al.*, *Curr. Biol.* **11**, 620 (2001).
- [6] H. Aizawa, *et al.*, *J. Cell. Biol.* **132**, 335 (1996).
- [7] T. Loisel, *et al.*, *Nature* **401**, 613 (1999).
- [8] A. Mogilner and L. Edelstein-Keshet, *Biophys. J.* **83**, 1237 (2002).
- [9] L. Edelstein-Keshet and G. Bard Ermentrout, *J. Math. Biol.* **43**, 325 (2001).
- [10] A. E. Carlsson, *Phys. Rev. Lett.*, **92**, 238102 (2004).
- [11] A. E. Carlsson, *Biophys. J.* **89**, 130 (2005).
- [12] A.E. Carlsson, *et al.*, *Biophys. J.* **86**, 1074 (2004).
- [13] A. E. Carlsson, *Biophys. J.* **90**, 413 (2006).
- [14] K. Kruse *et al.*, *Phys. Biol.* **3**, 130 (2006).
- [15] A. Mogilner and G. Oster, *Biophys. J.* **84**, 1591 (2003).
- [16] D. Pantaloni, *et al.*, *Nature Cell Biol.* **2**, 385 (2000).
- [17] A.M. Weaver *et al.*, *Curr. Biol.* **11**, 370 (2001).
- [18] K. Moriyama and I. Yahara, *EMBO J.* **18**, 6752 (1999).
- [19] I. Ichetovkin, *et al.*, *Curr. Biol.* **12**, 79 (2002).
- [20] T.D. Pollard and G.G. Borisy, *Cell* **112**, 453 (2003).
- [21] D. Vavylonis, *et al.*, *PNAS* **102**, 8543 (2005).
- [22] H.N. Higgs, *et al.*, *Biochemistry* **38**, 15212 (1999).
- [23] J.R. Kuhn and T.D. Pollard, *Biophys. J.* **88**, 1387 (2005).
- [24] J. Du and C. Frieden, *Biochemistry* **37**, 13276 (1998).
- [25] R. Melki, *et al.*, *Biochemistry* **35**, 12038 (1996).
- [26] K.-C. Lee and Andrea J. Liu (unpublished).
- [27] L. Blanchoin, *et al.*, *Nature* **404**, 1007 (2000).
- [28] I. Maly and G. Borisy, *PNAS* **98**, 11324 (2001).
- [29] M. Bailly, *et al.* *J. Cell. Biol.* **145**, 221 (1999).
- [30] D. Zicha, *et al.*, *Science* **300**, 142 (2003).
- [31] T. Svitkina, *et al.*, *J. Cell Biol.* **145**, 1009 (1999).